https://doi.org/10.5194/egusphere-2026-4039
Preprint. Discussion started: 29 July 2026

Measurement Report：Vertical New Particle Formation Profile observed at 356m Shenzhen Meteorological Tower

Yuting Li[1], Hao Wu[1*],Hancheng Hu[1],Yinshan Yang[2] , Youbiao Shi[3]

[1]Key Laboratory of China Meteorological Administration Atmospheric Sounding, School of Electrical Engineering, Chengdu University of Information Technology, Chengdu 610225, China
[2]Advanced Interdisciplinary Institute of Satellite Applications, Faculty of Geographical Science, Beijing Normal University, Beijing 100875 China;
[3]Kunming Lantian Meteorological Information Co., Ltd，Kunming 650000 China

Correspondence to: Hao Wu(wuhao@cuit.edu.cn)

Abstract. Vertical measurements of New Particle Formation (NPF) are essential yet scarce for understanding the role of ultrafine particles in lower boundary layer atmospheric processes. This study presents comprehensive vertical observations conducted at the 356m Shenzhen Meteorological Tower, utilizing mobility particle size spectrometers (SMPS and Nano-SMPS) at five heights (5-350 m) during two intensive observation periods (IOPs) in 2023. Results reveal distinct vertical dependencies in NPF characteristics. The NPF occurrence frequency was higher at ground level, while the particle growth rate (GR) was significantly enhanced aloft, increasing from 9 ± 4 nm h^{-1} at the surface to 14 ± 4 nm h^{-1} at 320 m. The vertical structure of NPF was classified into four types, which were closely related to the condensation sink (CS) higher at ground 0.04 s^{-1} than aloft 0.02 s^{-1}. Turbulence promoted near-surface nucleation with peak growth rates up to ~13 nm h^{-1} (average 9±4 nm h^{-1} at 5 m) and enhanced growth in the middle layers with GR values of 7–8 nm h^{-1} at 100–200 m (e.g., 8 nm h^{-1} at 100 m and 200 m, and 5–8 nm h^{-1} at 150 m), while growth rate at 350 m was mostly within 4 nm h^{-1}. Furthermore, the upper tower environment contributed more effectively to the conversion of new particles into cloud condensation nuclei, as supported by the significantly higher GR at 320 m (14±4 nm h^{-1}) compared to the surface (9±4 nm h^{-1}), indicating that particles aloft can grow into CCN active sizes more rapidly despite weaker turbulence at the highest levels. This work provides critical insights into aerosol vertical transport process and CCN production in the urban boundary layer.

https://doi.org/10.5194/egusphere-2026-4039
Preprint. Discussion started: 29 July 2026

Keywords: Meteorological tower; Vertical distribution; New particle formation; Turbulence

1 Introduction

Atmospheric aerosols, particularly ultrafine particles (UFPs, diameter < 100 nm), exert significant influence on global climate radiative forcing, cloud microphysics, and public health (Morawska et al., 2008;WHO, 2021; Jiang et al., 2023;Gong et al., 2025).A major source of UFPs is new particle formation (NPF), a process wherein gaseous precursors nucleate to form stable clusters that subsequently grow into larger particles (Kulmala et al., 2022;Coşgun et al., 2026;Ćirović et al., 2026;Gao et al., 2025). NPF contributes substantially to the global aerosol number budget and serves as a vital source of cloud condensation nuclei (CCN), thereby influencing cloud properties and precipitation patterns (Pöhlker et al., 2016; Williamson et al., 2019; Svensmark et al., 2017). In urban environments, NPF can exacerbate haze pollution through the rapid growth of newly formed particles (Chu et al., 2021;Wang et al., 2020;Du et al., 2021;Brean et al., 2024;Yang et al. 2026) and has been linked to adverse health outcomes due to the high deposition efficiency of UFPs in the human respiratory tract (Jiang et al., 2023; Dong et al., 2021; Ma et al., 2022).

The NPF process is governed by a complex interplay of factors including the abundance of precursor gases (e.g., sulfuric acid, volatile organic compounds VOCs), the pre-existing aerosol surface area acting as a condensation sink (CS), atmospheric oxidants (OH, O_3, NO_3), and meteorological conditions (Li et al., 2020; Fan et al., 2022;Flueckiger & Petrucci, 2024;Vidović et al., 2024;Zhang et al., 2026;Li et al., 2024). Recent studies emphasize the "air pollution complex" framework, where interactions between multiple pollutants and meteorology drive aerosol formation and evolution (Zhu et al., 2023). Key precursors like biogenic VOCs (BVOCs) and their oxidation products (oxidized organic molecules, OOMs) are increasingly recognized as critical drivers for particle nucleation and growth, especially in forested and urban areas (Zhao et al., 2020; Guo et al., 2020;Jin et al., 2025;Li et al., 2023).

While extensive ground-based observations have characterized NPF in diverse environments worldwide (Wu et al., 2021; Song et al., 2010; O'Donnell et al., 2023; Carnerero et al., 2018;Wang et al., 2025;Rowell et al., 2024;Kammer et al., 2023), the vertical dimension of NPF remains less understood due to measurement challenges. The atmospheric boundary layer (ABL) is highly stratified,

https://doi.org/10.5194/egusphere-2026-4039
Preprint. Discussion started: 29 July 2026

with strong gradients in precursor concentrations, aerosol properties, temperature, humidity, and dynamics (Lei et al., 2021). Turbulent mixing plays a pivotal role in vertically redistributing heat, moisture, trace gases, and aerosols, thereby modulating the microphysical and chemical environment for NPF. Consequently, NPF characteristics including its occurrence frequency, nucleation rate, particle growth rate (GR), and contribution to CCN can exhibit significant variability with height (Boulon et al., 2011;Leng et al., 2014; Yue et al., 2011).

Meteorological towers provide a unique and stable platform for investigating vertically resolved processes within the ABL. Studies conducted on towers in Beijing, the Amazon, and the Southern Great Plains have revealed profound vertical heterogeneity in aerosol composition, secondary formation, and the impact of vertical transport (Wang et al., 2016; Li et al., 2022; Chen et al., 2018). For instance, research in Beijing has shown that vertical mixing can amplify regional haze by elevating ground-level emissions and promoting particle growth aloft (Du et al., 2021). Other work has highlighted the importance of nitrate radical chemistry aloft (Fan et al., 2022;Yin et al., 2026) and the vertically resolved chemistry of primary and secondary aerosols (Lei et al., 2021). These findings underscore that ground observations alone may insufficiently represent the integrated column processes governing aerosol lifecycles and their climatic effects.

The Shenzhen Meteorological Tower (SZMGT), standing at 356 m, is among the tallest meteorological observation towers in Asia and offers an exceptional opportunity to study coastal urban atmospheric processes. Previous research utilizing this tower has investigated the vertical distribution of black carbon (Liang et al., 2022), PM2.5, O_3, and NOx (Li et al., 2020), as well as the vertical profile and sources of non-methane hydrocarbons (Mo et al., 2022). These studies confirm the presence of strong vertical gradients and the influence of both local emissions and regional transport in the Pearl River Delta region. However, a systematic, Multi-parameter investigation focusing specifically on the vertical characteristics of NPF and its controlling mechanisms at this location is still lacking.

This study aims to fill this critical knowledge gap by leveraging comprehensive vertical measurements conducted at the SZMGT across two intensive observational periods. We integrate state-of-the-art instrumentation for measuring particle size distributions (including nano and fine particles), chemical composition (VOCs, OOM proxies), key gaseous precursors, and turbulent parameters. We focus on quantifying and comparing the occurrence frequency, duration, and growth rates of NPF events at

https://doi.org/10.5194/egusphere-2026-4039
Preprint. Discussion started: 29 July 2026

multiple heights from the surface to 350 m, classifying the vertical structure types of NPF events in relation to the condensation sink and turbulent kinetic energy, elucidating the role of turbulent transport and mixing in modulating the vertical distribution of precursors, nucleation, and particle growth, examining the vertical profiles of key chemical drivers such as VOC oxidation products (OOM proxies) and their connection to particle growth dynamics, and finally assessing the implications of vertically varying NPF processes for the potential contribution of new particles to CCN populations in the urban boundary layer.

By providing a holistic, vertically resolved perspective on NPF in a rapidly developing coastal megacity, this work delivers critical insights into aerosol formation mechanisms. The findings are expected to enhance the mechanistic understanding of aerosol lifecycle in the urban boundary layer and support the improvement of aerosol representation in regional and global climate models.

2 Methodology

2.1 Measurement site

The Shenzhen meteorological tower with a height of 356 m is the tallest meteorological in Asia, located in the Shiyan Meteorological Observatory (113.91°E, 22.66°N) near to the Shenzhen airport (10 km to the west). The Tower provides 13 vertically distributed observation platforms (at 10, 20, 40, 50, 80, 100, 150, 160, 200, 250,300, 320, and 350m) .As the reservoir is an important source of drinking water for residents of Shenzhen, the environment within 1 km around the SZMGT is protected and rarely disturbed by human activity, ensuring that the underlying surface will remain natural for a long time.

https://doi.org/10.5194/egusphere-2026-4039
Preprint. Discussion started: 29 July 2026

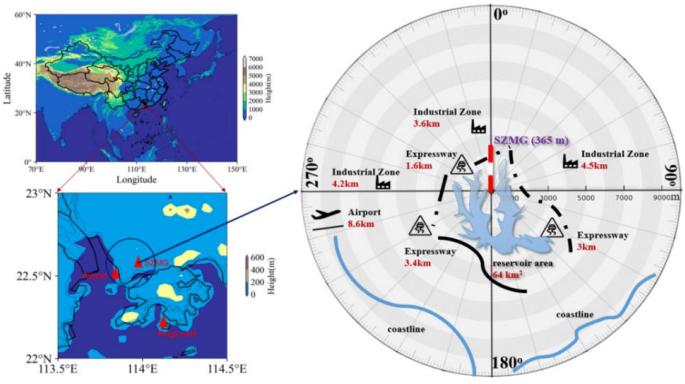

107

108 **Fig. 1 Tower location and the surroundings Geographical distribution pattern map**

109 Approximately 800 m north-east of the Shiyan Reservoir, there is a busy highway from
110 which vehicular pollutant emissions may influence the measurements on the tower. There is also
111 an airport located 10 km west of the base which serves an estimated 356000 flights in a normal
112 year. As such, the departure and arrival of airplanes at the airport may also potentially influence
113 pollutant concentration measurements by the SZMT. as it is located in a water source protection
114 area and surrounded by a litchi forest.

115 **2.2 Instrumentation**

116 **2.2.1 1st Intensity Observation Period （2023.3.1-2023.10.16）**

117 The SZMGT is 356 m tall, contains 13 layers of meteorological observation platforms that
118 begin from 10 to 350 m, Particle number size distributions between 1.8 nm and 500 nm were
119 monitored continuously by a Meteorological by a Vaisala WMT700 ultrasonic wind sensor and a
120 Vaisala HMP155 humidity and temperature probe.BNU SMPS system consisted of a long DMA
121 with a model 3772 CPC and the Nano-SMPS system consisted of a nano-DMA with a model 3776
122 ultrafine CPC. The measurement cycle for the SMPS and Nano-SMPS was 5 min, and the sample
123 flow was dried using a Nafion dryer. Electrical mobility sizing uncertainty is ±1%, verified by
124 poly-styrene latex aerosol size calibration standards, obtained every 5 minutes.Observation cabins,
125 gradient sampling systems and high-altitude sampling ports were set up at the Shenzhen
126 Meteorological Tower (SZMG). Vocus PTR and conventional instruments were used to observe
127 components such as volatile organic compounds (VOCs), NOx, O3 and CO.

https://doi.org/10.5194/egusphere-2026-4039
Preprint. Discussion started: 29 July 2026

2.2.2 2nd IOP （2023.09.18-10.27）

To confirm the consistency between nano SMPS and SMPS and the fixed reference instrument, an instrument comparison was conducted on the ground from September 18th to October 27th, 2023, serving as the reference instrument. Both have a good correlation with THU and use the corresponding slopes for data scaling.From October 14th to 26th, 2023, five observation points were set up on the tower at different heights, and various instruments were deployed for comprehensive monitoring: a Bi SMPS was equipped at 320 meters for high-precision aerosol particle counting and analysis; Equipped with NanoSMPS at 200 meters, it focuses on the detection of nanoscale particles. A common SMPS was set up at 150 meters to monitor particles in the medium particle size range. Another Bi SMPS was installed at a distance of 100 meters for particle measurement within the conventional particle size range. At the bottom of the tower (5 meters), TDMA is configured for monitoring low-concentration or settled particles. This hierarchical instrument system is designed to comprehensively analyze the distribution and dynamic changes of aerosol particles at different heights around the tower.

https://doi.org/10.5194/egusphere-2026-4039
Preprint. Discussion started: 29 July 2026

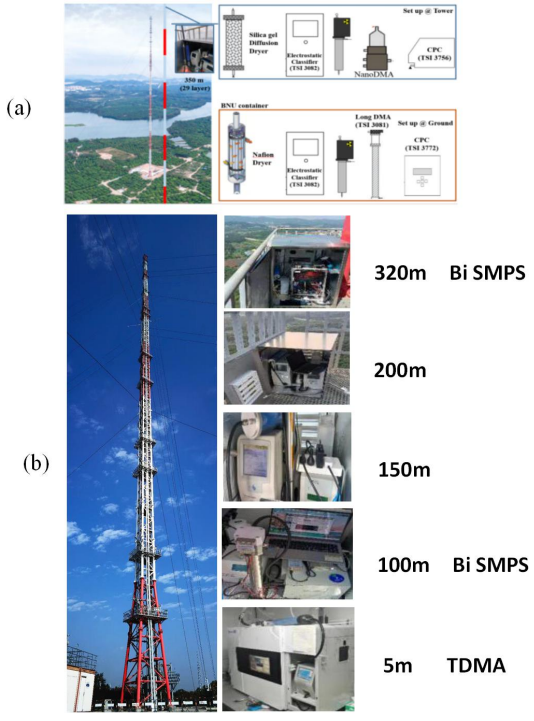

Fig. 2 （a）1st IOP. Instrument set up on the tower and ground.

(b)2nd IOP. Comprehensive monitoring by multiple instruments at five observation points.

2.3 Method

To delve into the characteristics of new particle formation (NPF) in the vertical dimension of the Shenzhen Tower, this study adopted and refined the methodologies from prior authoritative research. The aim was to quantify the key parameters associated with NPF, thereby ensuring consistency and comparability with existing literature.

2.3.1 NPF event classification

Firstly, all sampling days were classified according to the characteristics of the observed particle size distribution (PNSD) in relation to NPF events. In accordance with internationally recognized criteria (Dada et al., 2017; Kulmala et al., 2012;Lian et al., 2026), the sampling days were categorized into NPF event days, undefined days, and non - NPF days. The determination of an NPF event day requires the fulfillment of two core criteria simultaneously: the occurrence of

https://doi.org/10.5194/egusphere-2026-4039
Preprint. Discussion started: 29 July 2026

explosive growth of nucleation - mode particles (particle diameter < 25 nm) and the continuous growth of particle diameters over several hours, presenting a distinct growth trajectory (a typical "banana - shaped" growth curve). If a nucleation event takes place at noon but lacks prominent growth characteristics, or if the explosive growth of nucleation - mode particles occurs in the evening, the day is classified as an undefined day. Days with no observable nucleation or growth phenomena are designated as non - NPF days.

2.3.2 The calculation of the condensation sink (CS)

The condensation sink (CS), a crucial parameter that describes the capacity of existing particulate matter to scavenge condensable vapors, is calculated based on the measured dry particle number size distribution (PNSD). Here, i represents the particle size range index, $D_{p,i}$ represents the particle size, N_i represents the particle number concentration, D represents the condensation vapor diffusion coefficient, and β represents the correction factor.

$$CS = 2\pi \sum_i D\beta D_{p,i} N_i \quad (1)$$

2.3.3 sulfuric acid concentration proxy

Given the challenges associated with directly measuring gaseous sulfuric acid (SA) owing to its extremely low concentration in the atmosphere, this study employed two alternative strategies developed by Petäjä et al. (2009)

$$[H_2SO_4] = k\frac{[SO_2]*UVB}{CS} \quad (2)$$

These proxy metrics are derived from more readily measurable components. Their formulas are expressed as functions of the number concentrations of sulfuric acid (H2SO4) and sulfur dioxide (SO2) (in units of cm^{-3}) and ultraviolet B radiation (280 - 320 nm, in units of W m^{-2}). To calibrate the calculated SA values to match the measured ones, a constant k (9.9*10-7) was applied, as explicitly specified in the original formula.

2.3.4 The calculation of growth rate (GR)

https://doi.org/10.5194/egusphere-2026-4039
Preprint. Discussion started: 29 July 2026

The particle growth rate (GR) was computed using the modal fitting approach and is characterized as the rate of change of the modal particle diameter dp with respect to time (ddp/dt). Based on the time - resolved particle size distribution (PNSD) data, the representative modal dp was determined through log - normal distribution fitting (Hussein et al., 2005).

$$GMD = \exp\left(\frac{\sum (\ln d_{p,i}) \cdot N_i}{\sum N_i}\right) \quad (3)$$

The lognormal fitting of time-varying GMD was performed by the least square method (Kulmala et al., 2005) to obtain the particle size growth slope within a specific period:

$$GR = \frac{\Delta GMD}{\Delta t} \quad (4)$$

Among them, dp and i represent the diameters of the is the particle size, and N_i represents the corresponding concentration. This method quantifies the time-varying growth characteristics of the geometric mean diameter of the particle swarm.

2.3.5 The duration of the NPF event

The duration of new particle formation (NPF) events was determined based on the concentration of the nucleation mode. The start time was defined as the instant when the nucleation - mode concentration first intersects the threshold line and remains above it for 12 consecutive data points. The peak time corresponds to the point at which the nucleation - mode concentration reaches its maximum value. The end time was identified as the first secondary minimum point that occurs after the concentration drops below the threshold line. At this stage, due to the sharp decline in particle number concentration, the NPF event can no longer be differentiated from the background aerosol. This approach is consistent with the methods described by Dada et al. (2018) and Hakala et al. (2019).

2.3.6 Calculation of turbulent kinetic energy (TKE) and dissipation rate (ε)

The horizontal wind speed time series data U(z,t) (z represents height and t represents time) were obtained by using a three-dimensional ultrasonic anemometer (sampling frequency 10 Hz)

https://doi.org/10.5194/egusphere-2026-4039
Preprint. Discussion started: 29 July 2026

installed at a height of 320 meters on the tower and a wind lidar at the base of the tower (sampling frequency 0.2 Hz, vertical resolution 30 meters, maximum detection height 3 kilometers). The raw data underwent strict quality control: first, outliers were removed using the 3 times standard deviation criterion, and data with a single wind speed profile missing rate exceeding 20% (below 500 meters) were discarded; for the error caused by the installation tilt angle of the ultrasonic anemometer, the coordinate axes were corrected using the double rotation method. The above quality control process was repeated three times without data interpolation during the process.

2.3.7 Turbulent power spectrum and power-law index calculation

Perform Fourier transform on the wind speed sequence after quality control to obtain the turbulence power spectrum $P_z(f)$:

$$P_Z(f) = a\varepsilon^{\frac{2}{3}} f^n \quad (5)$$

Here, f represents the frequency, a is the Kolmogorov constant, ε is the dissipation rate, and n is the power-law index of the turbulence spectrum.(Kolmogorov, 1991; Kolmogorov, 1941)To solve n, take logarithmic linearization of the formula:

$$\log(P_Z(f)) = \log(a\varepsilon^{\frac{2}{3}}) + n\log(f) \quad (6)$$

Let $x = \log(f), b = \log(a\varepsilon^{\frac{2}{3}})$, and simplify it to:

$$\log(P_Z(f)) = b + nx \quad (7)$$

In the double logarithmic coordinate system, a linear fit is performed between $\log(f)$ and $\log(P_Z(f))$, with the slope being n. According to the characteristics of the instruments, the ultrasonic anemometer adopts a 2^{14} point FFT (27 minutes window), while the wind lidar adopts a 2^8 point FFT (20 minutes window). And based on the Nyquist sampling theorem, the effective frequency range is limited (ultrasonic anemometer ≤5 Hz, wind lidar ≤0.1 Hz). To enhance the temporal resolution, slide the FFT window at a 5-second step for calculation.

https://doi.org/10.5194/egusphere-2026-4039
Preprint. Discussion started: 29 July 2026

2.3.8 Inversion of turbulent kinetic energy and dissipation rate

Turbulent kinetic energy (TKE) can be obtained by integrating the power spectral density within a specific frequency range:

$$TKE = \sum P_Z(f) \quad (8)$$

Combining the n and TKE obtained through fitting, the dissipation rate ε is inversely solved from the power spectrum formula.This method reveals the evolution characteristics of the turbulent structure within the boundary layer through the vertical variation of the power-law exponent n, providing key turbulent parameter support for studying the vertical transport process of new particle generation.

2.3.9 Calculation of OOMS

The Precursor with an initial concentration of $[\mathrm{Precursor}]_0$ is continuously injected through flow F and is consumed by reacting with $O_3$and OH (generating OOMs), and is diluted with the gas flow (at a rate of $\frac{F}{V}*[P\mathrm{recursor}]_t$). When the system reaches a steady state, the rate of change of the precursor concentration over time is 0. At this point, the amount of the injected precursor is in balance with the amount consumed and diluted, that is:

$$\frac{\mathrm{F}}{\mathrm{V}}*[P\mathrm{recursor}]_0 = (k_{O_3}*[O_3]+k_{OH}*[OH]+\frac{F}{V})*[\mathrm{Pr}\,ecursor]_t \quad (9)$$

At this point, the rate at which the precursor is consumed by the oxidant (O_3, OH) is:

$$P_{OOM} = k_{O_3}*[O_3]*[\mathrm{Pr}\,ecursor]_t + k_{OH}*[OH]*[\mathrm{Precursor}]_t \quad (10)$$

It is equal to the generation rate of OOMs - because the reaction between precursors and oxidants is the sole source of OOMs (Lian et al., 2023).

3 Results I: 1st IOP（2023.3.1-2023.10.16）

https://doi.org/10.5194/egusphere-2026-4039
Preprint. Discussion started: 29 July 2026

3.1 The incidence rate and temporal variation characteristics of NPF events

During the 116-day intensive observation period of the 1st IOP, a total of 21 clear NPF events were observed at the upper level (on the tower), with an NPF occurrence frequency of 18%, while 30 clear NPF events were observed on the ground, with an NPF occurrence frequency of 26%, indicating that the ground atmosphere is more conducive to the occurrence of NPF. The monitoring data of SMPS from June 10, 2023 to June 17, 2023 were extracted for weekly variation study (Figure 3). It is not difficult to see that aerosol particles show obvious dynamic changes at different altitude layers. The active period for gas-phase precursor reactions and aerosol generation is at noon, during which micro-particles on the tower become concentrated and surge. Ground data also show significant fluctuations in concentration, and the peak value is higher than that on the tower, indicating that the accumulation and concentration of particles in the ground layer are higher. This vertical distribution feature indicates that there is a distinct vertical transport and diffusion process of aerosols during the day. Under the combined effect of meteorological conditions and pollution sources, it promotes the generation, growth and deposition of particles.

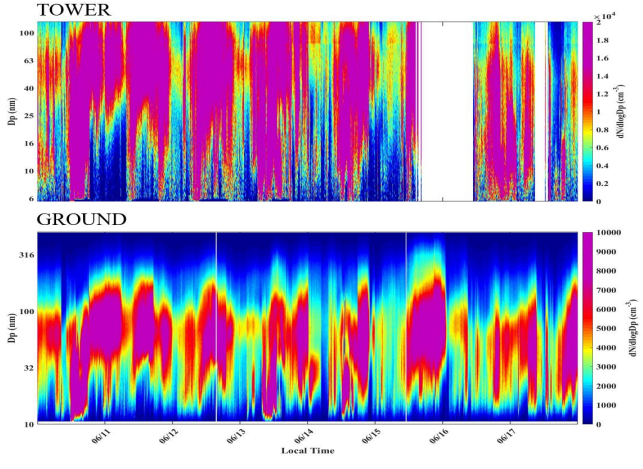

Figure 3.Weekly variations on the tower and the ground

3.2 NPF types on vertical scale

According to the NPF happens level, we have summary into four types(Figure 4), type A is the NPF both observed at ground and tower at the same day , type B is only happen on the ground,

https://doi.org/10.5194/egusphere-2026-4039
Preprint. Discussion started: 29 July 2026

269 and type C is NPF only happened on the tower,type D is the decreasing mode diameter event.

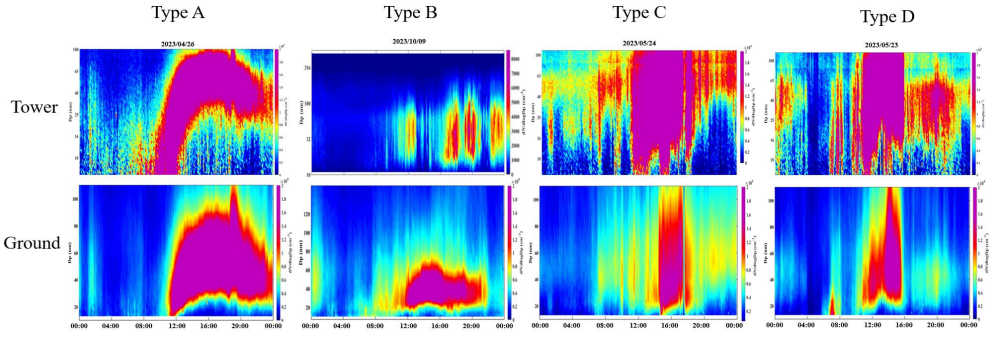

270

271 **Figure 4. Comparison of different NPF types**

272 Figure 5 shows the analysis of the CS box plot based on NPF types. There are significant
273 differences in CS corresponding to different NPF types. Type B (ground-only NPF) exhibits the
274 highest CS values with a median of approximately 0.04 s^{-1} (0.03–0.06 s^{-1}), while Type N
275 (non-NPF days) shows comparably high CS with a median around 0.055 s^{-1} (0.04–0.07 s^{-1}),
276 indicating that elevated pre-existing aerosol surface area suppresses NPF or limits its vertical
277 extension. In contrast, Type C (tower-only NPF) and Type D (decreasing mode diameter events)
278 display substantially lower CS medians of approximately 0.015 s^{-1} (0.01–0.02 s^{-1}) and 0.015 s^{-1}
279 (0.01–0.025 s^{-1}), respectively, consistent with the cleaner aloft environment (0.02 s^{-1}) that favors
280 nucleation aloft. Type A (simultaneous ground and tower NPF) shows a median CS of about 0.02
281 s^{-1} (0.01–0.04s^{-1}), suggesting that turbulent vertical mixing transports freshly nucleated particles
282 and precursors from the surface (with higher CS) to higher levels, effectively diluting the surface
283 CS influence aloft. Type U (undefined days) falls between ground and tower types with a median
284 CS of approximately 0.035 s^{-1} (0.025–0.05 s^{-1}), reflecting transitional conditions. Based on these
285 CS distributions, we infer that Type A is primarily influenced by turbulent vertical transport,
286 which spreads freshly nucleated particles and NPF precursors from the surface layer to higher
287 levels in the mixed layer (consistent with horizontal advection as an alternative mechanism). Type
288 C is driven by vertical mixing that brings precursors aloft while surface CS remains high, and
289 Type D is associated with the sinking of air masses that carry particles downward, leading to a
290 decrease in mode diameter.

https://doi.org/10.5194/egusphere-2026-4039
Preprint. Discussion started: 29 July 2026

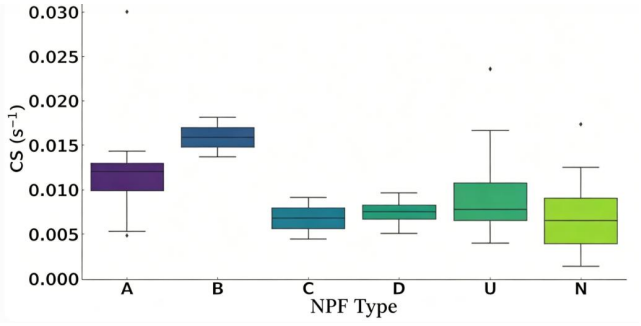

Figure 5. The mean CS level based on NPF types

From the corresponding contour heatmaps in Figure 6, it can be seen that the daily variation trends of these hydrocarbon species' concentrations at different heights (5 m, 40 m, 70 m, 120 m, 220 m, 335 m) are similar, but the concentration values vary significantly, with near-surface peak concentrations 1.3–2.8 times higher than those at the 335 m top layer. In most cases, there are peaks and troughs in the concentrations within a day, and the times when the concentration highs and lows occur at different heights are roughly the same, although the concentration fluctuation amplitude above 200 m decreases by over 60% compared with the surface layer. Other compounds such as isoprene, ethanol, and acetone show complex concentration distribution patterns with changes in height and time: isoprene high values are confined below 100 m during daytime, ethanol high-concentration plumes extend vertically up to 300 m, and acetone concentration peaks appear at the mid-layer of 100–200 m, indicating that the concentration distribution of these compounds in the vertical space not only varies with time but also has significant differences among different height levels. Overall, there are obvious differences in the concentrations of hydrocarbon species at different heights, suggesting that height is an important factor influencing the concentrations of hydrocarbon species. This may be related to multiple factors such as the diurnal evolution of the atmospheric boundary layer, vertical diffusion conditions, the vertical distribution of pollution sources, and height-dependent chemical reaction rates. For instance, lower heights (below 100 m) may be directly affected by ground-level source emissions, resulting in relatively higher concentrations; while higher heights above 200 m may be influenced by atmospheric transport and dilution, leading to more complex concentration variation patterns with weaker diurnal swings.

https://doi.org/10.5194/egusphere-2026-4039
Preprint. Discussion started: 29 July 2026

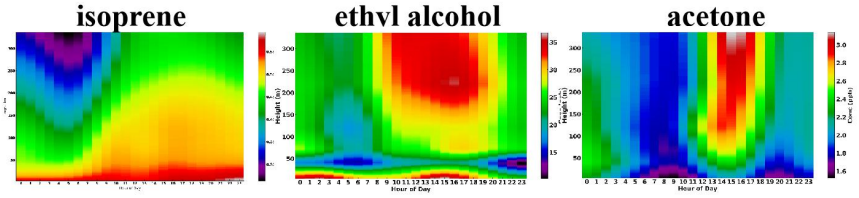

Figure 6.The diurnal variation results on 7/Apr/2023

Biogenic volatile organic compounds (BVOCs, such as isoprene and monoterpenes) are important substances emitted by plants. Their oxidation products can form new particles in the atmosphere, affecting clouds and climate. OOMs are the products of the reaction between precursors (BVOCs) and atmospheric oxidants (O_3, OH), and their generation rate can be deduced from the consumption process of the precursors. By monitoring the changes in precursor concentration over time, combined with the reaction rate constant and oxidant concentration, the generation rate of OOMs can be quantitatively calculated through the above formula (Figure 7).

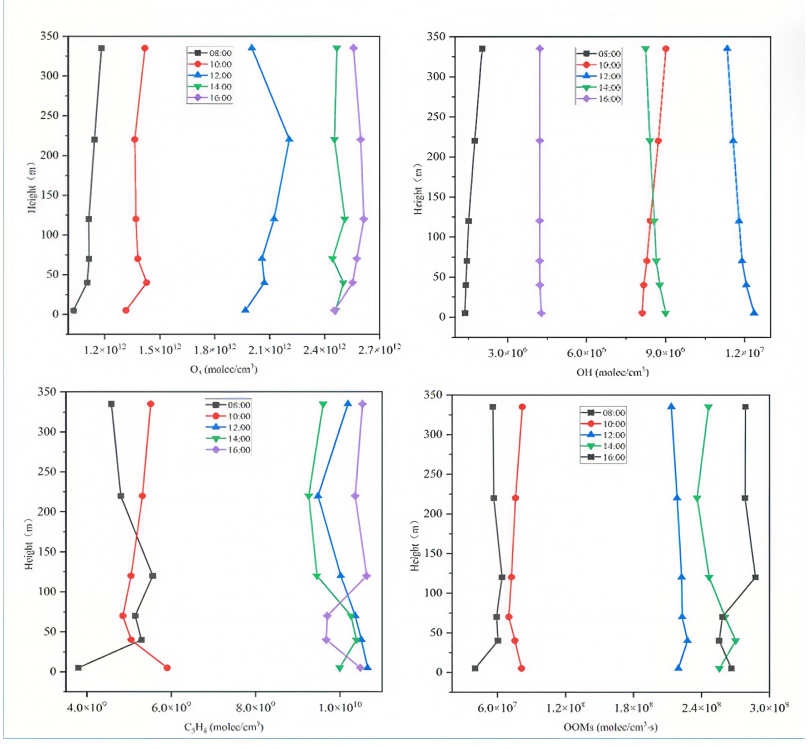

https://doi.org/10.5194/egusphere-2026-4039
Preprint. Discussion started: 29 July 2026

Figure 7.(a), (b), and (c) are the quantities required for calculating the OOMs.(d)The distribution relationship between the generation rate of OOMs and the corresponding height

Figure 7 presents the distribution relationship between the generation rate of oxidized organic molecules (OOMs) and the corresponding heights at different times (08:00, 10:00, 12:00, 14:00, 16:00). The research monitoring results show that: The generation rate of OOMs at noon (12:00 and 14:00) was significantly higher than that in the early morning, morning and evening, reaching a peak of (2.4×10^{8}) molec/cm³· s, and the corresponding height distribution was concentrated in the middle and upper layers (50-300 m), indicating that the photochemical reaction was more active at noon. Drive OOMs to generate efficiently and transmit to high altitudes; The peak generation rate of OOMs (6.0×10^{7} molec/cm³·s) is relatively low in the early morning (08:00), morning (10:00), and evening (16:00), and the height distribution is mainly near the ground to the middle and lower layers (0-200 m), reflecting the weak photochemical intensity during the non-midday period. The generation and vertical diffusion of OOMs are limited. The generation rate of OOMs in each period shows a single-peak variation with height. The peak height is related to the intensity of sunlight and the development of the boundary layer. Essentially, it is the result of the combined effect of photochemical oxidation intensity (driving the generation of OOMs) and atmospheric vertical diffusion (determining the height distribution). The temporal and vertical transport characteristics of the oxidation process of biogenic volatile organic compounds (VOCs) were verified.

4 2nd IOP (2023.10.14-10.26)

4.1The influence of turbulence on NPF

In the atmospheric boundary layer, turbulent transport has a profound impact on NPF. Turbulence can promote the mixing and exchange of substances at different elevation layers, transporting precursors, aerosols, etc. emitted by surface sources to the upper atmosphere, providing a material basis for NPF. Meanwhile, the dynamic disturbances caused by turbulence can alter the conditions of microphysical processes such as particle collisions and condensation, affecting the nucleation and growth of new particles. To clarify the effect of turbulent transport at different heights of the Shenzhen Tower on NPF, the second phase (2nd IOP) observation was carried out. Figure 8 focus on the temporal and spatial distribution of particle spectral diameters

https://doi.org/10.5194/egusphere-2026-4039
Preprint. Discussion started: 29 July 2026

(10-700 nm, 7-65nm, 13-500nm, 13-700nm, 10-532nm) and number concentrations at five heights (320m, 200m, 150m, 100m, 5m) .

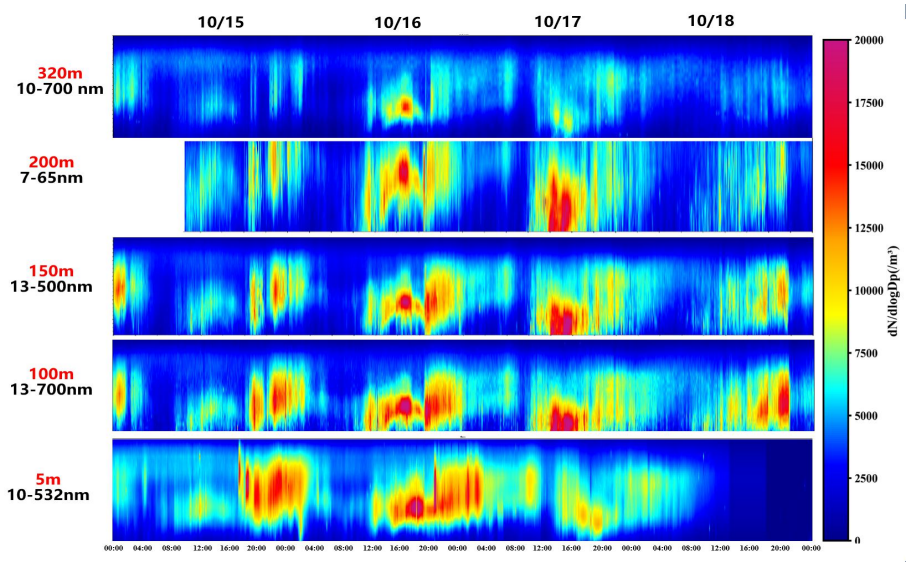

Figure 8.Particle spectral diameters at five heights (320m, 200m, 150m, 100m, 5m)

The second phase of observations at the Shenzhen Tower indicates that turbulent transport significantly affects NPF at different heights and shows a stratified pattern: near the ground (5m), turbulence accumulates surface precursor substances and promotes local reactions, serving as the "initial field" for new particle formation; at the middle and lower levels (100m, 150m, 200m), turbulence, with its active material transport and dynamic disturbances, either accelerates the formation and growth of new particles (e.g., efficient precursor transport at 200m) or regulates the formation-dissipation dynamics (e.g., at 100m); at the upper level (320m), weak turbulence only has a "limited triggering" effect on NPF. The vertical gradient characteristics of particle size distribution and number concentration changes at various heights clearly demonstrate the transition from near-ground accumulation to "weak response at high altitudes" driven by turbulence, providing multi-level observational evidence for understanding the turbulent regulation mechanism of new particle formation in the urban boundary layer. Further analysis on the data and concluded that turbulent vertical mixing promotes the development of the boundary layer, thereby resulting in a higher particle growth rate (GR). The GR data at different heights

https://doi.org/10.5194/egusphere-2026-4039
Preprint. Discussion started: 29 July 2026

(100m, 150m, 200m, 350m) and different dates (10.16 - 10.26, distinguished by legend colors) on the horizontal axis (unit: nm/h) verify the manifestation of this process at different vertical heights(Figure 9).

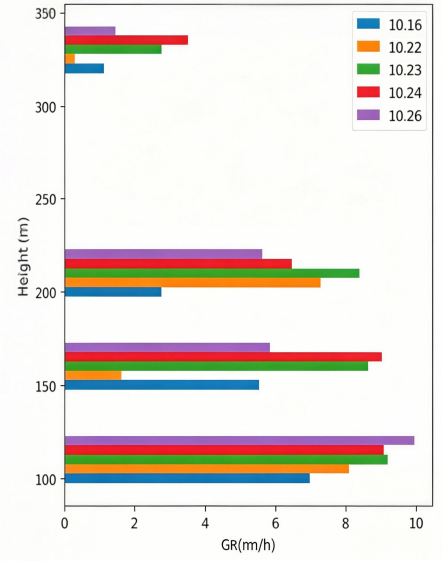

Figure 9.GR data at different heights

At a height of 100m, GR is relatively concentrated and has a high value. On some dates (such as 10.22 in orange and 10.23 in green), GR approaches or exceeds 8 nm/h. This indicates that the vertical mixing effect of turbulence near the ground (relatively low altitude) is significant, and the development of the boundary layer strongly promotes particle growth, which is conducive to the rapid growth of new particles. This may be due to the abundance of near-ground sources and the thorough mixing and reaction of precursors with particles caused by turbulence. At a height of 150m, the distribution of GR varies. For example, on 10.16 (blue, 5 nm/h) and 10.23 (green, exceeding 8 nm/h), the intensity of vertical mixing of turbulence and the degree of boundary layer development at this height change with meteorological conditions, affecting the fluctuation of particle growth rate, reflecting the dynamic regulation of GR by the middle atmosphere process. At a height of 200m, GR is mostly at a medium to high level on most dates (such as 10.22 in orange, exceeding 7 nm/h, and 10.23 in green,8 nm/h). This indicates that the vertical mixing of turbulence at this height continuously promotes the development of the boundary layer, providing

https://doi.org/10.5194/egusphere-2026-4039
Preprint. Discussion started: 29 July 2026

a stable environment for particle growth, and the transport and reaction conditions of precursors are well-matched, maintaining a relatively high GR. At a height of 350m, GR is generally lower than at the lower and middle altitudes (within 4 nm/h). This suggests that the vertical mixing of turbulence at high altitudes is relatively weak, and the promotion of particle growth by the development of the boundary layer is limited, resulting in a decrease in the particle growth rate, reflecting the attenuation of turbulence and boundary layer effects with increasing vertical height.

4.2 Turbulence associated with the PNSD

In the atmospheric environment, there is also a close connection between turbulence and the particle number size distribution (PNSD). On the one hand, turbulent motion can promote the mixing and diffusion of aerosol particles, redistributing particles of different sources and sizes in space. On the other hand, strong turbulence can increase the movement speed and collision frequency of particles, thereby accelerating the process of small particles growing into larger ones through condensation, and thus changing the shape and characteristics of the PNSD.

Take October 23 as an example. During the NPF event(Figure 13), at a height of 150 - 250 meters, the turbulent kinetic energy (TKE) rose from 0.5 m^2/s^3 to 3.0 m^2/s^3, and the dissipation rate increased from 0.01 m^2/s^3 to 0.1 m^2/s^3. The turbulent energy dissipation increased dramatically, and the movement was extremely active from the ground to the upper air. At the same time, the PNSD showed that the particle number concentration in the intermediate particle size range rose rapidly from about 2000 particles/cm^3 (light blue area) to about 12000 particles/cm^3. This indicates that the development of turbulence drives the dynamic changes of the PNSD by intensifying energy exchange and material transport. That is, active turbulence provides conditions for particle mixing and growth, significantly increasing the particle number concentration of specific particle sizes.

https://doi.org/10.5194/egusphere-2026-4039
Preprint. Discussion started: 29 July 2026

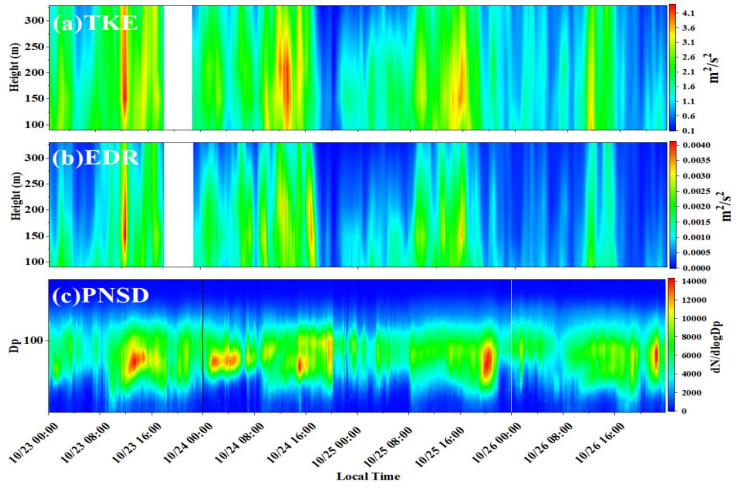

Figure 10.(a) Turbulent Kinetic Energy（TKE）（b）Energy Dissipation Rate（EDR）

(c) Particle Number Size Distribution（PNSD）

5 Conclusion

Based on multi-height observations at the Shenzhen Meteorological Tower (356 m, 10–350 m), this study reveals height-dependent NPF characteristics coupled with precursors, turbulence, and transformation. NPF occurrence was higher at ground (26%, 30 events) than aloft (18%, 21 events), while GR increased from 9±4 nm h^{-1} at surface to 14±4 nm h^{-1} at 320 m, confirming turbulent mixing attenuation with height. GR–CS correlation was stronger aloft, with ground CS higher (0.04 s^{-1}) than tower (0.02 s^{-1}). Turbulence driving particle growth via energy and mass exchange: near-surface promotes nucleation (GR up to 13 nm h^{-1}); middle layers (100–200 m) enhance precursor transport, TKE 0.5–3.0 m^2 s^{-3}, EDR 0.01–0.1 m^2 s^{-3}, and particle number increased 2000–12000 cm^{-3}; at 320 m. Photochemistry peaks at noon creat maximizing OOM production at 2.4×10^8 molec cm^{-3} s^{-1} (50–300 m) versus 6.0×10^7 during non-midday, promoting upward diffusion. Higher GR tower (14 to 9±4) allows faster growth to CCN-active sizes, making upper tower more effective for CCN conversion despite weaker turbulence.

Data availability. The vertical particle size distribution, trace gas, and turbulence datasets used in this study are available from the Mendeley Data repository (https://doi.org/10.17632/2t7ccgs762.1,

https://doi.org/10.5194/egusphere-2026-4039
Preprint. Discussion started: 29 July 2026

last access: 13 July 2026).

Author contributions. YT and HW designed the study. HHC,YYS,SYB contributed to the observation data, provided experimental assistance, and analyzed the methodology. YT wrote the paper with input from all the other authors.

Competing interests. The contact author has declared that noneof the authors has any competing interests.

Disclaimer. Publisher's note: Copernicus Publications remainsneutral with regard to jurisdictional claims made in the text, pub-lished maps, institutional affiliations, or any other geographical rep-resentation in this paper. The authors bear the ultimate responsibil-ity for providing appropriate place names. Views expressed in thetext are those of the authors and do not necessarily reflect the viewsof the publisher.

Acknowledgements. This study was funded by the Sichuan Provincial Central Leading Local Science and Technology Development Special Project (2025ZYD0179), the "Challenge and Command" China Meteorological Administration (CMAJBGS202607),the Open Grants of China Meteorological Administration Radar Meteorology Key Laboratory (2025ZD02), the Innovation Fund of the Jilin Field Research Station for Cloud Physics, China Meteorological Administration/Jilin Provincial Key Laboratory of Weather Modification (M202504), and the Key Laboratory of Intelligent Meteorological Observation Technology, China Meteorological Administration (ZNGC2025MS21), the National Natural Science Foundation of China (42325501).

https://doi.org/10.5194/egusphere-2026-4039
Preprint. Discussion started: 29 July 2026

References

[1] Morawska, L., Ristovski, Z., Jayaratne, E. R., Keogh, D. U., and Ling, X.: Ambient nano and ultrafine particles from motor vehicle emissions: characteristics, ambient processing and implications on human exposure, Atmos. Environ., 42, 8113 – 8138, https://doi.org/10.1016/j.atmosenv.2008.06.041, 2008.

[2] World Health Organization: WHO global air quality guidelines: particulate matter (PM2.5 and PM10), ozone, nitrogen dioxide, sulfur dioxide and carbon monoxide, World Health Organization, Geneva, 2021.

[3] Jiang, Y., Chen, R., Peng, W., Luo, Y., Chen, X., Jiang, Q., Han, B., Su, G., Duan, Y., Huo, J., Qu, X., Fu, Q., and Kan, H.: Hourly ultrafine particle exposure and acute myocardial infarction onset: an individual-level case-crossover study in Shanghai, China, 2015 – 2020, Environ. Sci. Technol., 57, 1701–1711, https://doi.org/10.1021/acs.est.2c06651, 2023.

[4] Kulmala, M., Cai, R., Stolzenburg, D., Zhou, Y., Dada, L., Guo, Y., Yan, C., Petäjä, T., Jiang, J., and Kerminen, V.-M.: The contribution of new particle formation and subsequent growth to haze formation, Environ. Sci.: Atmos., https://doi.org/10.1039/d1ea00096a, 2022.

[5] Pöhlker, M. L., Pöhlker, C., Ditas, F., Klimach, T., Hrabe de Angelis, I., Araújo, A., Brito, J., Carbone, S., Cheng, Y., Chi, X., Ditz, R., Gunthe, S. S., Kesselmeier, J., Könemann, T., Lavrič, J. V., Martin, S. T., Mikhailov, E., Moran-Zuloaga, D., Rose, D., Saturno, J., Su, H., Thalman, R., Walter, D., Wang, J., Wolff, S., Barbosa, H. M. J., Artaxo, P., Andreae, M. O., and Pöschl, U.: Long-term observations of cloud condensation nuclei in the Amazon rain forest – part 1: aerosol size distribution, hygroscopicity, and new model parametrizations for CCN prediction, Atmos. Chem. Phys., 16, 15709–15740, https://doi.org/10.5194/acp-16-15709-2016, 2016.

[6] Williamson, C. J., Kupc, A., Axisa, D., Bilsback, K. R., Bui, T., Campuzano-Jost, P., Dollner, M., Froyd, K. D., Hodshire, A. L., Jimenez, J. L., Kodros, J. K., Luo, G., Murphy, D. M., Nault, B. A., Ray, E. A., Weinzierl, B., Wilson, J. C., Yu, F., Yu, P., Pierce, J. R., and Brock, C. A.: A large source of cloud condensation nuclei from new particle formation in the tropics, Nature, 574, 399–403, https://doi.org/10.1038/s41586-019-1638-9, 2019.

https://doi.org/10.5194/egusphere-2026-4039
Preprint. Discussion started: 29 July 2026

[7] Svensmark, H., Enghoff, M. B., Shaviv, N. J., and Svensmark, J.: Increased ionization supports growth of aerosols into cloud condensation nuclei, Nat. Commun., 8, 2199, https://doi.org/10.1038/s41467-017-02082-2, 2017.

[8] Chu, B., Dada, L., Liu, Y., Yao, L., Wang, Y., Du, W., Cai, J., Daellenbach, K. R., Chen, X., Simonen, P., Zhou, Y., Deng, C., Fu, Y., Yin, R., Li, H., He, X. C., Feng, Z., Yan, C., Kangasluoma, J., Bianchi, F., Jiang, J., Kujansuu, J., Kerminen, V. M., Petäjä, T., He, H., and Kulmala, M.: Particle growth with photochemical age from new particle formation to haze in the winter of Beijing, China, Sci. Total Environ., 753, 142207, https://doi.org/10.1016/j.scitotenv.2020.142207, 2021.

[9] Wang, D., Li, Q., Shen, G., Deng, J., Zhou, W., Hao, J., and Jiang, J.: Significant ultrafine particle emissions from residential solid fuel combustion, Sci. Total Environ., 715, 136992, https://doi.org/10.1016/j.scitotenv.2020.136992, 2020.

[10] Du, W., Dada, L., Zhao, J., Chen, X., Daellenbach, K. R., Xie, C., Wang, W., He, Y., Cai, J., Yao, L., Zhang, Y., Wang, Q., Xu, W., Wang, Y., Tang, G., Cheng, X., Kokkonen, T. V., Zhou, W., Yan, C., Chu, B., Zha, Q., Hakala, S., Kurppa, M., Järvi, L., Liu, Y., Li, Z., Ge, M., Fu, P., Nie, W., Bianchi, F., Petäjä, T., Paasonen, P., Wang, Z., Worsnop, D. R., Kerminen, V.-M., Kulmala, M., and Sun, Y.: A 3D study on the amplification of regional haze and particle growth by local emissions, npj Clim. Atmos. Sci., 4, https://doi.org/10.1038/s41612-020-00156-5, 2021.

[11] Dong, J., Li, J., Tian, L., and Tu, J.: Transport and deposition of ultrafine particles in the upper tracheobronchial tree: a comparative study between approximate and realistic respiratory tract models, Comput. Methods Biomech. Biomed. Eng., 24, 1125 – 1135, https://doi.org/10.1080/10255842.2020.1869220, 2021.

[12] Ma, L., Zhang, Y., Lin, Z., Zhou, Y., Yan, C., Zhang, Y., Zhou, W., Ma, W., Hua, C., Li, X., Deng, C., Qi, Y., Dada, L., Li, H., Bianchi, F., Petäjä, T., Kangasluoma, J., Jiang, J., Liu, S., Hussein, T., Kulmala, M., and Liu, Y.: Deposition potential of 0.003–10 microm ambient particles in the humidified human respiratory tract: contribution of new particle formation events in Beijing, Ecotoxicol. Environ. Saf., 243, 114023, https://doi.org/10.1016/j.ecoenv.2022.114023, 2022.

[13] Li, L., Lu, C., Chan, P.-W., Zhang, X., Yang, H.-L., Lan, Z.-J., Zhang, W.-H., Liu, Y.-W., Pan, L., and Zhang, L.: Tower observed vertical distribution of PM2.5, O3 and NOx in the Pearl

https://doi.org/10.5194/egusphere-2026-4039
Preprint. Discussion started: 29 July 2026

512 River Delta, Atmos. Environ., 220, 117083, https://doi.org/10.1016/j.atmosenv.2019.117083,
513 2020.
514 [14] Fan, M. Y., Zhang, Y. L., Lin, Y. C., Hong, Y., Zhao, Z. Y., Xie, F., Du, W., Cao, F., Sun, Y.,
515 and Fu, P.: Important role of NO3 radical to nitrate formation aloft in urban Beijing: insights from
516 triple oxygen isotopes measured at the tower, Environ. Sci. Technol., 56, 6870 – 6879,
517 https://doi.org/10.1021/acs.est.1c02843, 2022.
518 [15] Zhu, T., Tang, M., Gao, M., Bi, X., Cao, J., Che, H., Chen, J., Ding, A., Fu, P., Gao, J., Gao,
519 Y., Ge, M., Ge, X., Han, Z., He, H., Huang, R.-J., Huang, X., Liao, H., Liu, C., Liu, H., Liu, J.,
520 Liu, S. C., Lu, K., Ma, Q., Nie, W., Shao, M., Song, Y., Sun, Y., Tang, X., Wang, T., Wang, T.,
521 Wang, W., Wang, X., Wang, Z., Yin, Y., Zhang, Q., Zhang, W., Zhang, Y., Zhang, Y., Zhao, Y.,
522 Zheng, M., Zhu, B., and Zhu, J.: Recent progress in atmospheric chemistry research in China:
523 establishing a theoretical framework for the “air pollution complex”, Adv. Atmos. Sci.,
524 https://doi.org/10.1007/s00376-023-2379-0, 2023.
525 [16] Zhao, B., Shrivastava, M., Donahue, N. M., Gordon, H., Schervish, M., Shilling, J. E., Zaveri,
526 R. A., Wang, J., Andreae, M. O., Zhao, C., Gaudet, B., Liu, Y., Fan, J., and Fast, J. D.: High
527 concentration of ultrafine particles in the Amazon free troposphere produced by organic new
528 particle formation, Proc. Natl. Acad. Sci. U. S. A., 117, 25344 – 25351,
529 https://doi.org/10.1073/pnas.2006716117, 2020.
530 [17] Guo, S., Hu, M., Peng, J., Wu, Z., Zamora, M. L., Shang, D., Du, Z., Zheng, J., Fang, X.,
531 Tang, R., Wu, Y., Zeng, L., Shuai, S., Zhang, W., Wang, Y., Ji, Y., Li, Y., Zhang, A. L., Wang,
532 W., Zhang, F., Zhao, J., Gong, X., Wang, C., Molina, M. J., and Zhang, R.: Remarkable
533 nucleation and growth of ultrafine particles from vehicular exhaust, Proc. Natl. Acad. Sci. U. S. A.,
534 117, 3427–3432, https://doi.org/10.1073/pnas.1916366117, 2020.
535 [18] Wu, H., Li, Z., Jiang, M., Liang, C., and Cribb, M.: Contributions of traffic emissions and
536 new particle formation to the ultrafine particle size distribution in the megacity of Beijing, Atmos.
537 Environ., https://doi.org/10.1016/j.atmosenv.2021.118472, 2021.
538 [19] Song, M., Lee, M., Kim, J. H., Yum, S. S., Lee, G., and Kim, K.-R.: New particle formation
539 and growth in relation to vertical mixing and chemical species during ABC-EAREX2005, Atmos.
540 Res., 97, 359–370, https://doi.org/10.1016/j.atmosres.2010.04.013, 2010.

https://doi.org/10.5194/egusphere-2026-4039
Preprint. Discussion started: 29 July 2026

[20] O'Donnell, S. E., Akherati, A., He, Y., Hodshire, A. L., Shilling, J. E., Kuang, C., Fast, J. D., Mei, F., Schobesberger, S., Thornton, J. A., Smith, J. N., Jathar, S. H., and Pierce, J. R.: Look up: probing the vertical profile of new particle formation and growth in the planetary boundary layer with models and observations, J. Geophys. Res.-Atmos., 128, https://doi.org/10.1029/2022jd037525, 2023.

[21] Lei, L., Sun, Y., Ouyang, B., Qiu, Y., Xie, C., Tang, G., Zhou, W., He, Y., Wang, Q., Cheng, X., Fu, P., and Wang, Z.: Vertical distributions of primary and secondary aerosols in urban boundary layer: insights into sources, chemistry, and interaction with meteorology, Environ. Sci. Technol., 55, 4542–4552, https://doi.org/10.1021/acs.est.1c00479, 2021.

[22] Boulon, J., Sellegri, K., Hervo, M., Picard, D., Pichon, J. M., Fréville, P., and Laj, P.: Investigation of nucleation events vertical extent: a long term study at two different altitude sites, Atmos. Chem. Phys., 11, 5625–5639, https://doi.org/10.5194/acp-11-5625-2011, 2011.

[23] Leng, C., Zhang, Q., Tao, J., Zhang, H., Zhang, D., Xu, C., Li, X., Kong, L., Cheng, T., Zhang, R., Yang, X., Chen, J., Qiao, L., Lou, S., Wang, H., and Chen, C.: Impacts of new particle formation on aerosol cloud condensation nuclei (CCN) activity in Shanghai: case study, Atmos. Chem. Phys., 14, 11353–11365, https://doi.org/10.5194/acp-14-11353-2014, 2014.

[24] Yue, D. L., Hu, M., Zhang, R. Y., Wu, Z. J., Su, H., Wang, Z. B., Peng, J. F., He, L. Y., Huang, X. F., Gong, Y. G., and Wiedensohler, A.: Potential contribution of new particle formation to cloud condensation nuclei in Beijing, Atmos. Environ., 45, 6070 – 6077, https://doi.org/10.1016/j.atmosenv.2011.07.037, 2011.

[25] Wang, J., Krejci, R., Giangrande, S., Kuang, C., Barbosa, H. M., Brito, J., Carbone, S., Chi, X., Comstock, J., Ditas, F., Lavric, J., Manninen, H. E., Mei, F., Moran-Zuloaga, D., Pohlker, C., Pohlker, M. L., Saturno, J., Schmid, B., Souza, R. A., Springston, S. R., Tomlinson, J. M., Toto, T., Walter, D., Wimmer, D., Smith, J. N., Kulmala, M., Machado, L. A., Artaxo, P., Andreae, M. O., Petäjä, T., and Martin, S. T.: Amazon boundary layer aerosol concentration sustained by vertical transport during rainfall, Nature, 539, 416 – 419, https://doi.org/10.1038/nature19819, 2016.

[26] Li, Y., Du, A., Lei, L., Sun, J., Li, Z., Zhang, Z., Wang, Q., Tang, G., Song, S., Wang, Z., Wang, Z., and Sun, Y.: Vertically resolved aerosol chemistry in the low boundary layer of Beijing in summer, Environ. Sci. Technol., 56, 9312–9324, https://doi.org/10.1021/acs.est.2c02861, 2022.

https://doi.org/10.5194/egusphere-2026-4039
Preprint. Discussion started: 29 July 2026

571 [27] Chen, H., Hodshire, A. L., Ortega, J., Greenberg, J., McMurry, P. H., Carlton, A. G., Pierce, J.
572 R., Hanson, D. R., and Smith, J. N.: Vertically resolved concentration and liquid water content of
573 atmospheric nanoparticles at the US DOE Southern Great Plains site, Atmos. Chem. Phys., 18,
574 311–326, https://doi.org/10.5194/acp-18-311-2018, 2018.
575 [28] Liang, Y., Wu, C., Wu, D., Liu, B., Li, Y. J., Sun, J., Yang, H., Mao, X., Tan, J., Xia, R.,
576 Deng, T., Li, M., and Zhou, Z.: Vertical distributions of atmospheric black carbon in dry and wet
577 seasons observed at a 356-m meteorological tower in Shenzhen, South China, Sci. Total Environ.,
578 853, 158657, https://doi.org/10.1016/j.scitotenv.2022.158657, 2022.
579 [29] Mo, Z., Huang, S., Yuan, B., Pei, C., Song, Q., Qi, J., Wang, M., Wang, B., Wang, C., and
580 Shao, M.: Tower-based measurements of NMHCs and OVOCs in the Pearl River Delta: vertical
581 distribution, source analysis and chemical reactivity, Environ. Pollut., 292, 118454,
582 https://doi.org/10.1016/j.envpol.2021.118454, 2022.
583 [30] Petäjä, T., Mauldin, R. L., Kosciuch, E., Aalto, P., Nieminen, T., Sipilä, M., Riipinen, I.,
584 Kulmala, M., and Weber, R. J.: Sulfuric acid and OH concentrations in a boreal forest site, Atmos.
585 Chem. Phys., 9, 7435–7448, https://doi.org/10.5194/acp-9-7435-2009, 2009.
586 [31] Coşgun, M. S., Kalkavouras, P., Alver Şahin, Ü., Ayvaz, C., Çolak, Z., Uzun Ayvaz, B., Onat,
587 B., Mihalopoulos, N., and Harrison, R. M.: First insights into the new particle formation
588 mechanism in Istanbul, Environ. Pollut., 397, 128018,
589 https://doi.org/10.1016/j.envpol.2026.128018, 2026.
590 [32] Ćirović, Ž., Stojanović, D. B., Davidović, M., Onjia, A., Alastuey, A., and
591 Jovašević-Stojanović, M.: New particle formation and source apportionment of particle number
592 size distribution in the urban area of the city of Belgrade, Atmosphere, 17, 205,
593 https://doi.org/10.3390/atmos17020205, 2026.
594 [33] Wang, H. Q., Li, X. X., Wu, J., Wu, H., Li, Y., Liu, C., Ma, N., Zeng, P., He, X., Ran, J.,
595 Song, H., Huang, D., Ding, F., Liu, W., Cheng, H., and Jiang, J.: Characterization of particle
596 number size distribution and new particle formation in a highly-humid megacity Wuhan, central
597 China, Atmos. Environ., 360, 121455, https://doi.org/10.1016/j.atmosenv.2025.121455, 2025.
598 [34] Gong, Y. R., Ou, J. P., Hu, Q. H., Xing, C. Z., Zhu, Y. Z., Wan, Y. H., Wang, D. N., Zhang,
599 C., Guan, L. X., Feng, J. X., Ji, X. G., Wang, X. Q., and Liu, C.: Explosive growth characteristics

https://doi.org/10.5194/egusphere-2026-4039
Preprint. Discussion started: 29 July 2026

of 5.6–560 nm particles and deposition in human respiratory during spring in Yangtze River Delta region, China, J. Environ. Sci., 155, 372–381, https://doi.org/10.1016/j.jes.2025.09.006, 2025.

[35] Flueckiger, A. C., and Petrucci, G. A.: Effect of relative humidity on the rate of new particle formation for different VOCs, Atmosphere, 15, 480, https://doi.org/10.3390/atmos15040480, 2024.

[36] Yin, R., Wu, Q., He, X.-C., Zhang, R., Li, Y., Wu, J., Liao, H., Yan, S., Wang, X., Zheng, R., Nie, W., Yan, C., Worsnop, D. R., Kulmala, M., He, K., Jiang, J., and Xie, H.-B.: Field evidence of new particle formation assisted by iodic acid in northern coastal China, Environ. Sci. Technol., 60, 10940–10949, https://doi.org/10.1021/acs.est.6c02345, 2026.

[37] Brean, J., Rowell, A., Beddows, D. C. S., Weinhold, K., Mettke, P., Merkel, M., Tuch, T., Rissanen, M., Dal Maso, M., Kumar, A., Barua, S., Iyer, S., Karppinen, A., Wiedensohler, A., Shi, Z., and Harrison, R. M.: Road traffic emissions lead to much enhanced new particle formation through increased growth rates, Environ. Sci. Technol., 58, 10664 – 10674, https://doi.org/10.1021/acs.est.4c02816, 2024.

[38] Yang, C., Brean, J., Xu, W., Xu, L., Huang, W., Fan, X., Bianchi, F., Du, W., Lin, Z., Li, L., Chen, G., Zhang, Y., Cai, R., Chen, Y., Li, M., and Chen, J.: Anthropogenic oxygenated organic molecules dominate new particle growth in moderate-pollution urban China, Environ. Sci. Technol., 60, 6364–6377, https://doi.org/10.1021/acs.est.5c04892, 2026.

[39] Jin, J., Cai, R., Liu, Y., Yang, G., Li, Y., Li, C., Yao, L., Jiang, J., Zhang, X., and Wang, L.: Atmospheric new particle formation in the eastern region of China: an investigation on mechanism and influencing factors at multiple sites, Atmos. Chem. Phys., 25, 17125 – 17138, https://doi.org/10.5194/acp-25-17125-2025, 2025.

[40] Vidović, K., Hočevar, S., Grgić, I., Metarapi, D., Dominović, I., Mifka, B., Gregorič, A., Alfoldy, B., and Ciglenečki, I.: Do bromine and surface-active substances influence the coastal atmospheric particle growth?, Heliyon, 10, e28672, https://doi.org/10.1016/j.heliyon.2024.e28672, 2024.

[41] Zhang, R., Li, Y., Zhao, J., Aridjis-Olivos, B., Zhao, L., Kowalewski, V., Kabir, M., Johnson, N. M., Nielsen, E. R., Brooks, S. D., Zhang, Y., Vedlitz, A., Porter, W., North, S. W., Li, W., Young, M. W., Seinfeld, J. H., Wang, Y., and Wang, Y.: Detecting supramolecular organic

https://doi.org/10.5194/egusphere-2026-4039
Preprint. Discussion started: 29 July 2026

nanoparticles during heat wave, Science, 391, eady5192, https://doi.org/10.1126/science.ady5192, 2026.

[42] Rowell, A., Brean, J., Beddows, D. C. S., Shi, Z., Kumar, A., Rissanen, M., Dal Maso, M., Mettke, P., Weinhold, K., Merkel, M., and Harrison, R. M.: The behaviour of charged particles (ions) during new particle formation events in urban Leipzig, Germany, Atmos. Chem. Phys., 24, 10349–10361, https://doi.org/10.5194/acp-24-10349-2024, 2024.

[43] Lian, Y., Bai, X., Yuan, R., Wei, T., Mao, H., Peng, J., and Jiang, S.: Atmospheric aerosol nucleation: a methodological review of theoretical calculations and molecular simulation, Environ. Sci.: Atmos., 6, https://doi.org/10.1039/D6EA00026F, 2026.

[44] Li, D., Huang, W., Wang, D., Wang, M., Thornton, J. A., Caudillo, L., Rörup, B., Marten, R., Scholz, W., Finkenzeller, H., Marie, G., Baltensperger, U., Bell, D. M., Brasseur, Z., Curtius, J., Dada, L., Duplissy, J., Gong, X., Hansel, A., He, X.-C., Hofbauer, V., Junninen, H., Krechmer, J. E., Kürten, A., Lamkaddam, H., Lehtipalo, K., Lopez, B., Ma, Y., Mahfouz, N. G. A., Manninen, H. E., Mentler, B., Perrier, S., Petäjä, T., Pfeifer, J., Philippov, M., Schervish, M., Schobesberger, S., Shen, J., Surdu, M., Tomaz, S., Volkamer, R., Wang, X., Weber, S. K., Welti, A., Worsnop, D. R., Wu, Y., Yan, C., Zauner-Wieczorek, M., Kulmala, M., Kirkby, J., Donahue, N. M., George, C., El-Haddad, I., and Bianchi, F.: Nitrate radicals suppress biogenic new particle formation from monoterpene oxidation, Environ. Sci. Technol., 58, 1601 – 1614, https://doi.org/10.1021/acs.est.3c06271, 2024.

[45] Li, C., Li, Y., Li, X., Cai, R., Fan, Y., Qiao, X., Yin, R., Yan, C., Guo, Y., Liu, Y., Zheng, J., Kerminen, V.-M., Kulmala, M., Xiao, H., and Jiang, J.: Comprehensive simulations of new particle formation events in Beijing with a cluster dynamics–multicomponent sectional model, Atmos. Chem. Phys., 23, 6879–6896, https://doi.org/10.5194/acp-23-6879-2023, 2023.

[46] Kammer, J., Simon, L., Ciuraru, R., Petit, J.-E., Lafouge, F., Buysse, P., Bsaibes, S., Henderson, B., Cristescu, S. M., Durand, B., Fanucci, O., Truong, F., Gros, V., and Loubet, B.: New particle formation at a peri-urban agricultural site, Sci. Total Environ., 857, 159370, https://doi.org/10.1016/j.scitotenv.2023.159370, 2023.

[47] Gao, Z., Wang, F., Du, W., Wang, S., Sun, Y., Yang, W., Wang, X., Han, B., and Bai, Z.: Elucidating particle number concentrations and unveiling source mechanisms at a prominent

https://doi.org/10.5194/egusphere-2026-4039
Preprint. Discussion started: 29 July 2026

national background site on the northeastern Qinghai-Tibetan Plateau, Sci. Total Environ., 969, 178928, https://doi.org/10.1016/j.scitotenv.2025.178928, 2025.

[48] Kulmala, M., Petäjä, T., Nieminen, T., Aalto, P., Sipilä, M., Riipinen, I., Dal Maso, M., and Kerminen, V.-M.: Measurement of the nucleation rate of atmospheric nanoparticles: a review of methods and recent progress, Atmos. Chem. Phys., 12, 11267 – 11308, https://doi.org/10.5194/acp-12-11267-2012, 2012.

[49] Dada, L., Yan, C., Nie, W., Duplissy, J., Bianchi, F., Petäjä, T., and Kulmala, M.: New particle formation events in a polluted megacity (Beijing): seasonal variation and governing factors, Atmos. Chem. Phys., 17, 13061 – 13080, https://doi.org/10.5194/acp-17-13061-2017, 2017.

[50] Petäjä, T., Kerminen, V.-M., Paasonen, P., Aalto, P., Nieminen, T., Sipilä, M., Riipinen, I., Kulmala, M., and Weber, R. J.: Sulfuric acid and OH concentrations in a boreal forest site, Atmos. Chem. Phys., 9, 747–766, https://doi.org/10.5194/acp-9-747-2009, 2009.

[51] Hussein, K., Dal Maso, M., Petäjä, T., Aalto, P., Väkevä, M., and Kulmala, M.: Automated multi-lognormal fitting of atmospheric particle number size distributions, Boreal Environ. Res., 10, 337–350, https://doi.org/10.3174/ber.10.3.337, 2005.

[52] Kulmala, M., Petäjä, T., Mönkkönen, P., Koponen, I. K., Dal Maso, M., Aalto, P. P., and Kerminen, V.-M.: On the growth of nucleation mode particles: source rates of condensable vapour in polluted and clean environments, Atmos. Chem. Phys., 5, 409 – 422, https://doi.org/10.5194/acp-5-409-2005, 2005.

[53] Dada, L., Kangasluoma, J., Nieminen, T., Aalto, P., Yan, C., Petäjä, T., and Kulmala, M.: Refined classification and characterization of atmospheric new particle formation events using air ions, Atmos. Chem. Phys., 18, 14883–14905, https://doi.org/10.5194/acp-18-14883-2018, 2018.

[54] Hakala, S., Vakkari, V., Petäjä, T., Aalto, P., and Kulmala, M.: New particle formation, growth and apparent shrinkage at a rural background site in western Saudi Arabia, Atmos. Chem. Phys., 19, 10537–10555, https://doi.org/10.5194/acp-19-10537-2019, 2019.

[55] Kolmogorov, A. N.: The local structure of turbulence in incompressible viscous fluid for very large Reynolds numbers, Dokl. Akad. Nauk SSSR, 30, 299–303, 1941.

[56] Kolmogorov, A. N.: Local structure of turbulence at large Reynolds numbers, Phys.-Usp., 34, 425–433, https://doi.org/10.1070/PU1991v034n05ABEH002497, 1991.